WARWICK
THE UNIVERSITY OF WARWICK

Original citation:
Koh, Ming Liang, FitzGerald, Paul A., Warr, Gregory G., Jolliffe, Katrina A. and Perrier, Sébastien. (2016) Study of (cyclic peptide)-polymer conjugate assemblies by small-angle neutron scattering. Chemistry - A European Journal

Permanent WRAP URL:
http://wrap.warwick.ac.uk/83849

Copyright and reuse:
The Warwick Research Archive Portal (WRAP) makes this work by researchers of the University of Warwick available open access under the following conditions. Copyright © and all moral rights to the version of the paper presented here belong to the individual author(s) and/or other copyright owners. To the extent reasonable and practicable the material made available in WRAP has been checked for eligibility before being made available.

Copies of full items can be used for personal research or study, educational, or not-for profit purposes without prior permission or charge. Provided that the authors, title and full bibliographic details are credited, a hyperlink and/or URL is given for the original metadata page and the content is not changed in any way.

Publisher's statement:
This is the peer reviewed version of the following article: Koh, M. L., FitzGerald, P. A., Warr, G. G., Jolliffe, K. A. and Perrier, S. (2016), Study of (Cyclic Peptide)–Polymer Conjugate Assemblies by Small-Angle Neutron Scattering. Chem. Eur. J.. doi:10.1002/chem.201603091, which has been published in final form at http://dx.doi.org/10.1002/chem.201603091 . This article may be used for non-commercial purposes in accordance with Wiley Terms and Conditions for Self-Archiving."

A note on versions:
The version presented here may differ from the published version or, version of record, if you wish to cite this item you are advised to consult the publisher's version. Please see the 'permanent WRAP url' above for details on accessing the published version and note that access may require a subscription.

For more information, please contact the WRAP Team at: wrap@warwick.ac.uk

warwick.ac.uk/lib-publications

Study of (cyclic peptide)-polymer conjugate assemblies by small angle neutron scattering

Ming Liang Koh,[1,2] Paul A. FitzGerald,[1] Gregory G. Warr,[1] Katrina A. Jolliffe,[1,*] Sébastien Perrier[1,2,3*]

[1] School of Chemistry, The University of Sydney, NSW 2006, Australia.

[2] Department of Chemistry, University of Warwick, Coventry CV4 7AL, United Kingdom.

[3] Faculty of Pharmacy and Pharmaceutical Sciences, Monash University, VIC 3052, Australia.

[*] Katrina A. Jolliffe, kate.jolliffe@sydney.edu.au; Sébastien Perrier, s.perrier@warwick.ac.uk

Abstract

We present a fundamental study into the self-assembly of (cyclic peptide)-polymer conjugates as a versatile supramolecular motif to engineer nanotubes with defined structure and dimensions, as characterised in solution using small angle neutron scattering (SANS). This work demonstrates the ability of the grafted polymer to stabilise and/or promote the formation of unaggregated nanotubes by the direct comparison to the unconjugated cyclic peptide precursor. This ideal case permitted a further study into the growth mechanism of self-assembling cyclic peptides, allowing an estimation of the cooperativity. Furthermore we show the dependency of the nanostructure on the polymer and peptide chemical functionality in solvent mixtures that vary in the ability to compete with the intermolecular associations between cyclic peptides and ability to solvate the polymer shell.

Keywords

cyclic peptide, polymer conjugates, RAFT polymerization, supramolecular, nanotubes, self-assembly

Graphical abstract

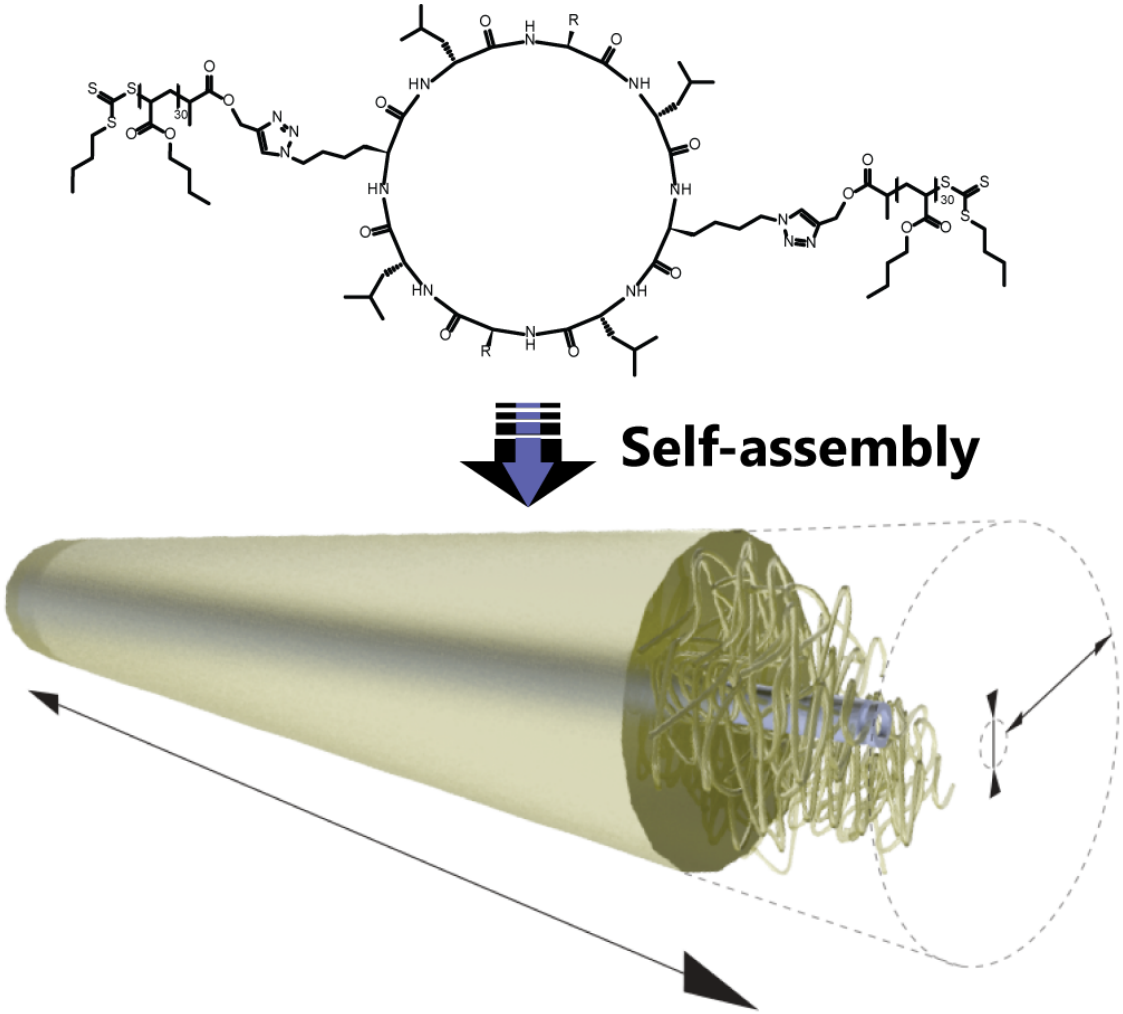

Introduction

Nanotubes are attractive scaffolds for a variety of applications such as materials, electronics, sensors, catalysis, drug delivery and ion channels, owing to their anisotropic geometry, rigid structure and their internal pore.[1-6] While there are covalent-based routes to tubular nanostructures, notably, bottlebrush copolymers[7-9] and carbon nanotubes,[10] the performance of natural systems such as gramicidin A,[11,12] α-hemolysin,[13] and the tobacco mosaic virus,[14,15] which are capable of precise manufacturing of nanotubes as well as enabling dynamic/reversible properties, are highly inspiring incentives for taking a supramolecular approach.

Self-assembly is a powerful route that has been used to realise synthetic structures with control on the nanometer length scale.[16] Pioneered in the 1990s, cyclic peptides (CPs) of alternating D and L amino acids adopt a conformation that promotes stacking between CP units by the formation of cylindrical *β*-sheets.[17,18] Many groups, including our own, have used self-assembling CPs as a guiding motif for nanotube structures. Self-assembling CPs are a highly versatile design platform[19] in which alterations to the CPs are reflected in the final cyclic peptide nanotube assembly; for example, the number of amino acids in the CP correlates to the diameter of the nanotube.[19] Since the earliest examples of self-assembling CPs, imaging techniques have shown the assemblies as very long and rigid structures,[17] yet controlling the length of the extended nanotube structures (i.e. beyond dimerisation) is not straightforward, requiring the self-assembly process to be tamed. However, in a recent example, Mizrahi *et al*. demonstrated length control through the use of a 'layer-by-layer'-like approach, where the authors sequentially deposited positively and negatively charged CPs to obtain short nanotubes of precise lengths.[20] An interesting templating approach was proposed by Granja *et al*., stemming from their molecular dynamics study of CPs (*α* and *γ* residues), they suggest that the use of organochloride molecules in a highly hydrogen bonding competitive solvent (such as water) would promote the association of the CPs around the guest molecule (i.e. enveloping the molecule in the core of the nanotube) and promote dissociation of the CPs beyond the chain length of the organochloride molecule.[21]

The conjugation of synthetic polymers to natural products, particularly biopolymers, is a simple and effective approach to combine functionalities which can be engineered for a multitude of applications.[22-24] Likewise the recent developments in covalent tethering synthetic polymers to self-assembling cyclic peptides[25-30] have further widened the possibilities by adding functionality for processing,[31,32] pH[33] or temperature[34,35] stimuli response, or for drug delivery.[36,37] Additionally the tethered polymers allow control over the

nanotubular structure such as the diameter,[38,39] ordering and orientation,[40] promoting formation of macropores,[41] or to stabilise the otherwise dynamic exchange of CPs[39,42]. In the context of controlling the nanotube length, Biesalski *et al*. first suggested the use of increasing the polymer mass and graft density to tailor the length of the nanotubes by steric repulsion.[25] These authors then investigated the impact of the polymer molecular mass by using atomic force microscopy to characterise the surface absorbed nanostructure (after drying) which showed an increase in height and decrease in nanotube length as the polymer molar mass increased.[38] Recently we reported the first characterisation of (cyclic peptide)-polymer assemblies in solution by the use of small angle neutron scattering (SANS), confirming their rigid rod structure and providing the dimensions of the assembly.[43] An interesting result of this study showed the impact of the grafted polymer length on the assembly structure in solution, revealing that the nanotube length depends on both steric hindrance and solvent accessibility to the peptide core, i.e. the increase of tethered polymer mass can promote the formation of tubes by shielding the CP core from a solvent that competes with the intermolecular H-bonding between CPs.[43]

Here we directly compare the supramolecular structures formed by non-conjugated CPs and polymer-conjugated CPs in solution by SANS, and also examine the influence of the solvating media by varying the strength of competition for H-bonding sites and polymer solvation. These conjugates present an ideal system by which to study the self-assembly of cyclic peptides, providing insight to the growth mechanism including an estimation of the degree of cooperativity. Variations to the cyclic peptide residues with polar and non-polar side chains also enable a study of the impact of chemical functionality at the external periphery of the peptide core.

Experimental Section

Equipment

Microwave-assisted copper(I) catalysed azide-alkyne cycloaddition (CuAAC) reactions were performed using a CEM Discover SP microwave reactor using 5 mL borosilicate microwave vessels.

Synthesis

Detailed synthetic methods can be found in the supplementary information. In brief: Fmoc-L-Lys(N_3)-OH was prepared from Fmoc-L-Lys-OH using a diazotransfer reagent[44,45] in a method described in literature.[27] 4-(4,6-Dimethoxy-1,3,5-triazin)-4-

methylmorpholinium tetrafluoroborate (DMTMM.BF_4) was prepared following literature procedures.[46] Linear octapeptides were synthesised by fluorenylmethyloxycarbonyl (Fmoc) solid phase peptide synthesis[47-49] using: 2-chlorotrityl chloride resin; Fmoc deprotection with piperidine/*N*,*N*-dimethylformamide (DMF) (1:4 v/v); amino acid coupling with HBTU/HATU, *N*,*N*-diisopropylethylamine (DIPEA), DMF; and cleaved from the resin with 1,1,1,3,3,3-hexafluoroisopropanol (HFIP)/dichloromethane (DCM) (1:4 v/v). Cyclic peptides were synthesised by the head-to-tail coupling of linear peptides as described below.

CP1. H_2N(-L-Lys(N_3)-D-Leu-L-Trp(Boc)-D-Leu)$_2$-OH (0.41 g, 0.31 mmol) was dissolved in DMF (20 mL) with 5 min of sonication. The solution was purged with $N_{2(g)}$ at room temperature, then cooled with an ice/water bath. DMTMM.BF_4 (0.12 g, 0.37 mmol) in DMF (5 mL) was purged with $N_{2(g)}$ and added dropwise to the linear peptide solution. The solution was brought to room temperature and stirred for 91 h under an atmosphere of $N_{2(g)}$. DMF was removed under reduced pressure. The residue was washed with ice-cold MeOH (4×20 mL) then dried under reduced pressure. Boc groups were removed by treatment with TFA/TIPS/H_2O (18:1:1 v/v/v, 5 mL) for 2 h, then the mixture was triturated with ice-cold diethyl ether and washed twice with ice-cold diethyl ether to give **CP1** as an off-white powder: 0.25 g, 71 % yield; ^{1}H NMR (400 MHz, TFA-*d*) δ ppm: 8.11 (d, J = 8 Hz, 2H, 2×Trp-$CH_{aromatic}$), 7.66 (d, J = 8 Hz, 2H, 2×Trp-$CH_{aromatic}$), 7.54 (s, 2H, 2×Trp-$CH_{aromatic}$), 7.26-7.42 (m, 4H, 4×Trp-$CH_{aromatic}$), 5.21 (t, J = 8 Hz, 2H, 2×Trp-α-H), 4.60-4.85 (br m, 6H, 4×Leu-α-H + 2×Lys(N_3)-α-H), 3.00-3.40 (br m, 8H, 2×Lys(N_3)-CH_2-N_3 + 2×Trp-α-CH_2), 0.50-2.00 (br m, 48H, 2×Lys(N_3)-α-CH_2-CH_2-CH_2 + 4×Leu-α-CH_2-CH + 8×Leu-CH_3); MALDI-FTICR MS m/z = 1156 $(M+Na)^+$; ATR-FTIR ν_{max} cm^{-1}: 3270 (N-H_{str}), 2093 (N_3), 1626 (C=O_{str}).

CP2. H_2N(-L-Lys(N_3)-D-Leu-L-Lys(Boc)-D-Leu)$_2$-OH (0.09 g, 0.08 mmol) was dissolved in DMF (73 mL) with 1 h of sonication at 40 °C. The solution was purged with $N_{2(g)}$. DMTMM.BF_4 (0.03 g, 0.09 mmol) in DMF (3 mL) was purged with $N_{2(g)}$ and added dropwise to the linear peptide solution. The solution was stirred for 67 h at 40 °C under an atmosphere of $N_{2(g)}$. DMF was removed under reduced pressure. The residue was washed with MeOH precooled to -78 ^{o}C (dry-ice/acetone) (2×10 mL) then dried under reduced pressure to give **CP2** as a white powder: 42 mg, 45 % yield; ^{1}H NMR (400 MHz, TFA-*d*); ^{1}H NMR (400 MHz, TFA-*d*) δ ppm: 4.60-5.00 (m, 8H, 2×Lys(N_3)-α-H + 2×Lys-α-H + 4×Leu-α-H), 3.41 (t, J = 6 Hz, 4H, 2×Lys(N_3)-CH_2-N_3), 3.20-3.34 (br m, 4H, Lys-CH_2-NH_2), 1.25-2.12 (br m, 36H, 2×Lys(N_3)-α-CH_2-CH_2-CH_2 + 2×Lys-α-CH_2-CH_2-CH_2 + 4×Leu-α-

CH_2-CH), 0.91-1.11 (br m, J = 8 Hz, 24H, 8×Leu-CH_3); ESI-LCQ MS m/z = 1240 $(M+Na)^+$; ATR-FTIR ν_{max} cm^{-1}: 3270 (N-H_{str}), 3037-2800 (C-H_{str}), 2096 (N_3), 1624 (C=O_{str}).

CP3. H_2N(-L-Lys(N_3)-D-Leu-L-Lys(Boc)-D-Leu)$_2$-OH (0.19 g, 0.15 mmol) was dissolved in DMF (142 mL) with 75 min of sonication at 40 °C. The solution was purged with $N_{2(g)}$. DMTMM.BF_4 (0.06 g, 0.18 mmol) in DMF (20 mL) was purged with $N_{2(g)}$ and added dropwise to the linear peptide solution. The solution was stirred for 67 h at 40 °C under an atmosphere of $N_{2(g)}$. DMF was removed under reduced pressure. Boc groups were removed by treatment with TFA/thioanisole/TIPS/H_2O (88:5:2:5vol, 20 mL) for 2 h, then the mixture was washed with acetic acid/diethyl ether precooled to -78 °C (dry-ice/acetone) (1:1 v/v, 2×40 mL), washed twice with diethyl ether precooled to -78 °C (dry-ice/acetone) (2×40 mL) and then dried under reduced pressure to give **CP3** as a white powder: 63 mg, 33 % yield; ^{1}H NMR (400 MHz, TFA-*d*) δ ppm: 4.75-5.15 (m, 8H, 2×Lys(N_3)-α-H + 2×Lys-α-H + 4×Leu-α-H), 3.56 (t, J = 8 Hz, 4H, 2×Lys(N_3)-CH_2-N_3), 3.33-3.50 (br m, 4H, Lys-CH_2-NH_2), 1.40-2.26 (br m, 36H, 2×Lys(N_3)-α-CH_2-CH_2-CH_2 + 2×Lys-α-CH_2-CH_2-CH_2 + 4×Leu-α-CH_2-CH), 1.17 (d, J = 8 Hz, 24H, 8×Leu-CH_3); MALDI-FTICR MS m/z = 1068 $(M-2N_2+Ag)^+$; ATR-FTIR ν_{max} cm^{-1}: 3273 (N-H_{str}), 3006-2790 (C-H_{str}), 2099 (N_3), 1627 (C=O_{str}).

CP-($NH_3.CF_3COO)_2$. H_2N(-L-Lys(Boc)-D-Leu-L-Trp(Boc)-D-Leu)$_2$-OH (1.00 g, 0.67 mmol) was dissolved in DMF (115 mL) with 10 min of sonication. The solution was purged with $N_{2(g)}$ at room temperature, then cooled with an ice/water bath. DMTMM.BF_4 (0.26 g, 0.8 mmol) in DMF (15 mL) was purged with $N_{2(g)}$ and added dropwise to the linear peptide solution. The solution was brought to room temperature and stirred for 6 d under an atmosphere of $N_{2(g)}$. DMF was removed under reduced pressure. The residue was suspended and washed with ice/water-cold MeOH (3×20 mL) then dried under reduced pressure. Cyclo[(-L-Lys(Boc)-D-Leu-L-Trp(Boc)-D-Leu)$_2$] (0.148 g, 0.099 mmol) was treated with TFA/TIPS/H_2O (18:1:1 v/v/v, 5 mL) for 2 h, then the mixture was triturated with diethyl ether precooled to -78 °C (dry-ice/acetone) and washed twice with diethyl ether precooled to -78 °C (dry-ice/acetone) to give cyclo[(-L-Lys-D-Leu-L-Trp-D-Leu)$_2$] as an off-white powder: 124 mg, 96 % yield; ^{1}H NMR (400 MHz, TFA-*d*) δ ppm: 8.13 (d, J = 8 Hz, 2H, 2×Trp-$CH_{aromatic}$), 7.65 (d, J = 8 Hz, 2H, 2×Trp-$CH_{aromatic}$), 7.55 (s, 2H, 2×Trp-$CH_{aromatic}$), 7.26-7.42 (m, 4H, 4×Trp-$CH_{aromatic}$), 5.22 (t, J = 8 Hz, 2H, 2×Trp-α-H), 4.60-4.87 (m, 6H, 4×Leu-α-H + 2×Lys-α-H), 3.04-3.37 (m, 8H, 2×Lys-CH_2-N + 2×Trp-α-CH_2), 0.55-2.00 (br m, 48H, 2×Lys-α-CH_2-CH_2-CH_2 + 4×Leu-α-CH_2-CH + 8×Leu-CH_3); ESI-ToF MS m/z = 1081.0 $(M+H)^+$; ATR-FTIR ν_{max} cm^{-1}: 3273 (N-H_{str}), 1627 (C=O_{str}).

r-terminal alkyne RAFT agent (propynyl 2-propanoate)yl butyl trithiocarbonate (PPBTC) was prepared following a similar protocol to that described previously.[50] *r*-terminal *N*-succinimidyl ester RAFT agent (NHS-PABTC) was prepared following a previously described protocol.[35,41] Polymers with α-alkyne and α-NHS functional group were synthesised by RAFT polymerisation.

Poly(*n*-butyl acrylate) with an alkyne end group was synthesised by RAFT polymerisation: PPBTC (0.25 g, 0.9 mmol), BA (3.9 g, 31.5 mmol) and AIBN (0.015 g, 0.09 mmol) was mixed and diluted to 40 % (w/w) with dioxane, cooled in an ice bath and purged with $N_{2(g)}$ for 15 min before stirring at 70 °C under an atmosphere of $N_{2(g)}$ until 79 % conversion determined by ^{1}H NMR. The polymer was precipitated and washed with ice-cold water/MeOH (1:9) to yield **pBA$_{30}$** as a yellow viscous liquid: M_n (^{1}H NMR) = 4200 g·mol^{-1}; ^{1}H NMR (400 MHz, $CDCl_3$) δ ppm: 4.78-4.88 (m, 1H, pBA-S-CH), 4.58-4.72 (m, 2H, $PPBTC_R$-COO-CH_2), 3.80-4.30 (m, 30×2H, pBA-COO-CH_2), 3.34 (t, J = 6 Hz, 2H, S-CH_2), 0.70-2.60 (m, 311H, $PPBTC_Z$-CH_2-CH_2-CH_3 + 30×pBA-CH_2-CH_2-CH_3 + 30×$pBA_{backbone}$-CH-CH_2 + $PPBTC_R$-CH_3 + $PPBTC_R$-C≡CH); SEC-DRI(DMF+LiBr): M_n = 3500 g·mol^{-1}, $Đ$ = 1.16. MALDI-ToF MS: $(M+Na)^+$ observed; repeat unit m/z = 128, end group m/z = 276.

Poly(*n*-butyl acrylate) with an *N*-succinimidyl ester end group was synthesised by RAFT polymerisation. NHS-PABTC (0.075 g, 0.22 mmol), BA (1.04 g, 7.8 mmol), ACVA (0.018 g, 0.0065 mmol) in dioxane (0.94 g) was purged with $N_{2(g)}$ for 15 min before stirring at 70 °C under an atmosphere of $N_{2(g)}$ until 94 % conversion determined by ^{1}H NMR. The polymer was twice precipitated and washed with water/MeOH (1:9) precooled to -78 ^{o}C (dry-ice/acetone) to yield **pBA$_{33}$** as a yellow viscous liquid: M_n (^{1}H NMR) = 4600 g·mol^{-1}; ^{1}H NMR (300 MHz, $CDCl_3$) δ ppm: 4.76-4.89 (br t, 1H, pBA-S-CH), 3.86-4.20 (m, 33×2H, pBA-COO-CH_2), 3.34 (t, J = 6 Hz, 2H, S-CH_2), 2.67-2.89 (m, 5H, NHS-CH_2-CH_2- + R-CH-COO), 0.66-2.67 (m, 339H, Z-CH_2-CH_2-CH_3 + 33×pBA-CH_2-CH_2-CH_3 + 33×$pBA_{backbone}$-CH-CH_2 + R-CH_3); SEC-DRI($CHCl_3$+TEA): M_n = 4700 g·mol^{-1}, $Đ$ = 1.09.

CP1-(pBA$_{30}$)$_2$ was synthesised following a previously described protocol.[29] **CP1** (40 mg, 0.035 mmol) was suspended in TFE (2 mL) by sonication for 10 min. **PBA$_{30}$** (0.31 g, 0.074 mmol), sodium ascorbate (0.14 g, 0.71 mmol) and $CuSO_4.5H_2O$ (0.037 g, 0.14 mmol) in DMF (3 mL) were added to the cyclic peptide solution, then the mixture was placed in a microwave reactor and irradiated (dynamic mode) at 100 °C for 15 min with a flow of $N_{2(g)}$ and delivering 200 W in the initial ramp. TFE and DMF were removed under reduced pressure. The crude product was dissolved in DCM and washed with an aqueous solution of EDTA (2×30 mL, 0.055 M, pH 8.5), then water (30 mL), and dried over $MgSO_4$. After

concentration *in vacuo*, **CP1-(pBA_{30})$_2$** was obtained as a brown film: 145 mg, 100 % conversion (ATR-FTIR); ^{1}H NMR (300 MHz, TFA-*d*) δ ppm: 8.48 (s, 2H, 2×triazole-CH), 7.60 (s, 2H, 2×Trp-$CH_{aromatic}$), 7.34 (s, 2H, 2×Trp-$CH_{aromatic}$), 7.02-7.26 (m, 6H, 6×Trp-$CH_{aromatic}$), 5.46 (s, 4H, 2×O-CH_2-triazole), 5.18 (s, 2H, 2×Trp-α-H), 4.52-4.87 (m, 6H, 4×Leu-α-H + 2×Lys-α-H), 4.24 (s, 64H, 32×pBA-O-CH_2), 3.95 (s, 2H, PPBTC$_z$-CH_2), 1.71 (s, 64H, 32×pBA- CH_2), 1.42 (s, 64H, 32×pBA-CH_2), 0.98 (s, 96H, 32×pBA-CH_3), 0.73-0.89 (m, 24H, 8×Leu-CH_3), 0.45 (d, J = 10.15 Hz, 3H, PPBTC$_r$-CH_3), 0.15-0.22 (m, 3H, PPBTCz-CH_3); ATR-FTIR ν_{max} cm^{-1}: 3274 (N-H_{str}), 3045-2750 (C-H_{str}), 1728 (C=$O_{p(BA)}$), 1625 (C=$O_{CP\text{-}str}$).

CP2-(pBA_{30})$_2$. **CP2** (10 mg, 0.008 mmol), **pBA_{30}** (0.071 g, 0.017 mmol), sodium ascorbate (0.016 g, 0.081 mmol) and $CuSO_4.5H_2O$ (0.009 g, 0.036 mmol) were suspended in DMF (3 mL), then the mixture was placed in a microwave reactor and irradiated (dynamic mode) at 100 °C for 15 min with a flow of $N_{2(g)}$ and delivering 200 W in the initial ramp. The DMF was removed under reduced pressure. In attempt to push the reaction to completion, a second microwave irradiation was performed after adding sodium ascorbate (0.016 g, 0.081 mmol) and $CuSO_4.5H_2O$ (0.009 g, 0.036 mmol) in DMF (3 mL). The crude product was dissolved in $CHCl_3$ and washed with an aqueous solution of EDTA (2×30 mL, 0.055 M, pH 8.5), then water (30 mL), and dried over $MgSO_4$. After concentration *in vacuo*, **CP2-(pBA_{30})$_2$** was obtained as a dark brown film: 54 mg, < 100 % conversion (ATR-FTIR); ATR-FTIR ν_{max} cm^{-1}: 3272 (N-H_{str}), 3040-2800 (C-H_{str}), 2098 (N_3), 1729 (C=$O_{p(BA)}$), 1624 (C=$O_{CP\text{-}str}$).

CP2-(pBA_{30})$_{1.5}$. **CP2** (5 mg, 0.004 mmol), **pBA_{30}** (0.024 g, 0.006 mmol), sodium ascorbate (0.008 g, 0.040 mmol) and $CuSO_4.5H_2O$ (0.005 g, 0.020 mmol) were suspended in DMF (2.5 mL), then the mixture was placed in a microwave reactor and irradiated (dynamic mode) at 100 °C for 15 min with a flow of $N_{2(g)}$ and delivering 200 W in the initial ramp. The DMF was removed under reduced pressure, then the crude product was dissolved in $CHCl_3$ and washed with an aqueous solution of EDTA (2×30 mL, 0.055 M, pH 8.5), then water (30 mL), and dried over $MgSO_4$. After concentration *in vacuo*, **CP2-(pBA_{30})$_{1.5}$** was obtained as a brown film: 20 mg, ≤ 100 % conversion (ATR-FTIR); ATR-FTIR ν_{max} cm^{-1}: 3270 (N-H_{str}), 3040-2800 (C-H_{str}), 2097 (N_3), 1732 (C=$O_{p(BA)}$), 1625 (C=$O_{CP\text{-}str}$).

CP3-(pBA_{30})$_2$. **CP3** (10 mg, 0.008 mmol), **pBA_{30}** (0.085 g, 0.021 mmol), sodium ascorbate (0.020 g, 0.098 mmol) and $CuSO_4.5H_2O$ (0.010 g, 0.039 mmol) were suspended in DMF (2 mL) then the mixtrue was placed in a microwave reactor and irradiated (dynamic mode) at 100 °C for 15 min with a flow of $N_{2(g)}$ and delivering 200 W in the initial ramp. The

DMF was removed under reduced pressure and the crude product was dissolved in DCM and washed with an aqueous solution of EDTA (2×30 mL, 0.055 M, pH 8.5), then water (30 mL), and dried over $MgSO_4$. After concentration *in vacuo*, **CP3-(pBA$_{30}$)$_2$** was obtained as a dark brown film: 52 mg, ≤ 100 % conversion (ATR-FTIR); ATR-FTIR ν_{max} cm^{-1}: 3279 (N-H$_{str}$), 3050-2800 (C-H$_{str}$), 1733 (C=O$_{p(BA)}$), 1631 (C=O$_{CP\text{-}str}$).

CP3-(pBA$_{30}$)$_{1.5}$. **CP3** (10 mg, 0.008 mmol), **pBA$_{30}$** (0.062 g, 0.015 mmol), sodium ascorbate (0.021 g, 0.11 mmol) and $CuSO_4.5H_2O$ (0.011 g, 0.042 mmol) were suspended in DMF (2 mL), then the mixture was placed in a microwave reactor and irradiated (dynamic mode) at 100 °C for 15 min with a flow of $N_{2(g)}$ and delivering 200 W in the initial ramp. The DMF was removed under reduced pressure. The crude product was dissolved in DCM and washed with an aqueous solution of EDTA (2×30 mL, 0.055 M, pH 8.5), then water (30 mL), and dried over $MgSO_4$. After concentration *in vacuo*, **CP3-(pBA$_{30}$)$_{1.5}$** was obtained as a dark brown film: 49 mg, ≤ 100 % conversion (ATR-FTIR); ATR-FTIR ν_{max} cm^{-1}: 3280 (N-H$_{str}$), 3060-2800 (C-H$_{str}$), 1733 (C=O$_{p(BA)}$), 1631 (C=O$_{CP\text{-}str}$).

CP-(pBA$_{33}$)$_2$ by NHS conjugation. Cyclo[(-L-Lys-D-Leu-L-Trp-D-Leu)$_2$] (0.020 g, 0.015 mmol), **pBA$_{33}$** (0.202 g, 0.044 mmol) and NMM (0.093 g, 0.092 mmol) were suspended in a mixture DMF/DMSO (1:3vol, 4 mL) and stirred for 4 days at room temperature. Solvents were removed with a stream of $N_{2(g)}$ and the product was redissolved in DCM, then precipitated into dry-ice/acetone-cold MeOH/H_2O (9:1vol). The precipitate was redissolved in THF and purified by preparative size exclusion using a column of Bio-Beads S-X1. Gravity flow elution permitted isolation of conjugate in the form of self-assembled structures as detected by laser light scattering and analysed by SEC(DMF). Concentrated *in vacuo*, **CP-(pBA$_{33}$)$_2$** was obtained as a yellow film: 9.7 mg, 100 % conversion (ATR-FTIR); M_p (SEC-DRI(DMF+NH_4BF_4)) = 6600 g.mol^{-1} (n.b. free polymer M_p 2900 g.mol^{-1}); ATR-FTIR ν_{max} cm^{-1}: 3276 (N-H$_{str}$), 3040-2800 (C-H$_{str}$), 1733 (C=O$_{p(BA)}$), 1624 (C=O$_{CP\text{-}str}$).

Small angle neutron scattering (SANS)

SANS measurements were performed on the NG3 beamline at the National Institute of Standards of Technology Center for Neutron Research in Gaithersburg, MD, USA. Raw data was corrected for detector sensitivity, background and empty cell scattering, and then converted to absolute scattered intensity ($d\Sigma/d\Omega$ cm^{-1}) from the absolute neutron flux.[51] Incident neutrons had an average wavelength of 6 Å and wavelength resolution $\Delta\lambda/\lambda = 0.124$. Sample-to-detector distances (SDD) of 1.33 m and 8 m were used and the data combined for

0.0057 $Å^{-1} \leq q \leq 0.43$ $Å^{-1}$. For **CP1-(pBA$_{30}$)$_2$** in THF-d_8 (2 mM), SDD of 1.33 m, 8 m, and 13.17 m were used and the data combined for 0.0030 $Å^{-1} \leq q \leq 0.43$ $Å^{-1}$. Hellma cells (2 mm path length) were used for data acquisition.

SANS sample preparation

CP1-pBA$_{30}$ (1 mM) samples in TFA-*d*/THF-d_8 (1:9 v/v and 9:1 v/v) and TFA-*d*/$CDCl_3$ (1:9 v/v and 9:1 v/v) mixtures were prepared from mixing appropriate volumes of **CP1-pBA$_{30}$** (1 mM in TFA-*d*), **CP1-pBA$_{30}$** (1 mM in THF) and **CP1-pBA$_{30}$** (1 mM in $CDCl_3$) then transferred to Hellma cells for data acquisition. An alternative sample preparation (as indicated in text), involving the solvent mixture TFA-*d*/THF-d_8 (1:9 v/v), was prepared by dissolving **CP1-pBA$_{30}$** in TFA-*d* and diluting with THF-d_8 (as opposed to mixing two solutions of **CP1-pBA$_{30}$**).

SANS analysis

Models incorporated in the NCNR analysis macro using IGOR Pro 6.34A were used to fit to the collected data.[51] The general procedure followed for fitting was to begin with a uniform, monodisperse, hard sphere model, then, where necessary, fit complexity was increased to consider polydisperse spheres, uniform ellipsoids, uniform cylinders, polydisperse cylinders, and core-shell cylinders to gain further insight. The parameters: scale (volume fraction), solvent SLD and incoherent background were always fixed while the other parameters were fit to the data. Repeated fittings with various manually input starting parameters were used to assess the validity of the fit. Solvent SLDs were determined from literature values of scattering lengths and cross sections[52] using the NCNR SLD calculator,[53] and SLDs of solvent mixtures were determined by weighted averages. Where removed, incoherent scattering was subtracted using the Porod Law ($I(q)\cdot q^4$ vs q^4 plot).[54]

Static light scattering (SLS)

SLS experiments were performed on an ALV-CGS3 goniometer system. A 633 nm, vertically polarised laser was used, and the sample was kept at 20 °C throughout the experiment. Dark count rate was recorded at 90°, distilled and filtered toluene ($n = 1.491$, $R_\theta = 1.35 \times 10^{-5}$) was used to calibrate the instrument, and filtered THF ($n = 1.409$) was used as a blank for background subtraction. **CP-(pBA$_{33}$)$_2$** in THF (2 mM) was prepared with filtered THF (but the sample was not filtered) and analysed in a quartz cell at angles 15°-149° taking 3×10 sec intensity measurements at 2° increments.

Results and Discussion

A range of self-assembling cyclic peptides (**CP1-3**) containing azide moieties were obtained by Fmoc- solid phase peptide synthesis (SPPS) and poly *n*-butyl acrylates containing an alkyne functional group at the α-terminus were prepared using reversible addition-fragmentation chain transfer (RAFT) polymerisation. The peptide polymer conjugates were then prepared by reaction of minimal excess polymer, CPs and polymers in a microwave-assisted copper(I) catalysed azide-alkyne cycloaddition (CuAAC) using a high concentration of copper catalyst (Scheme 1), following a previously published procedure.[29] The cyclic peptides (CPs) and the cyclic-peptide polymer conjugates were then examined using SANS to determine the structure of the assemblies formed in solution.

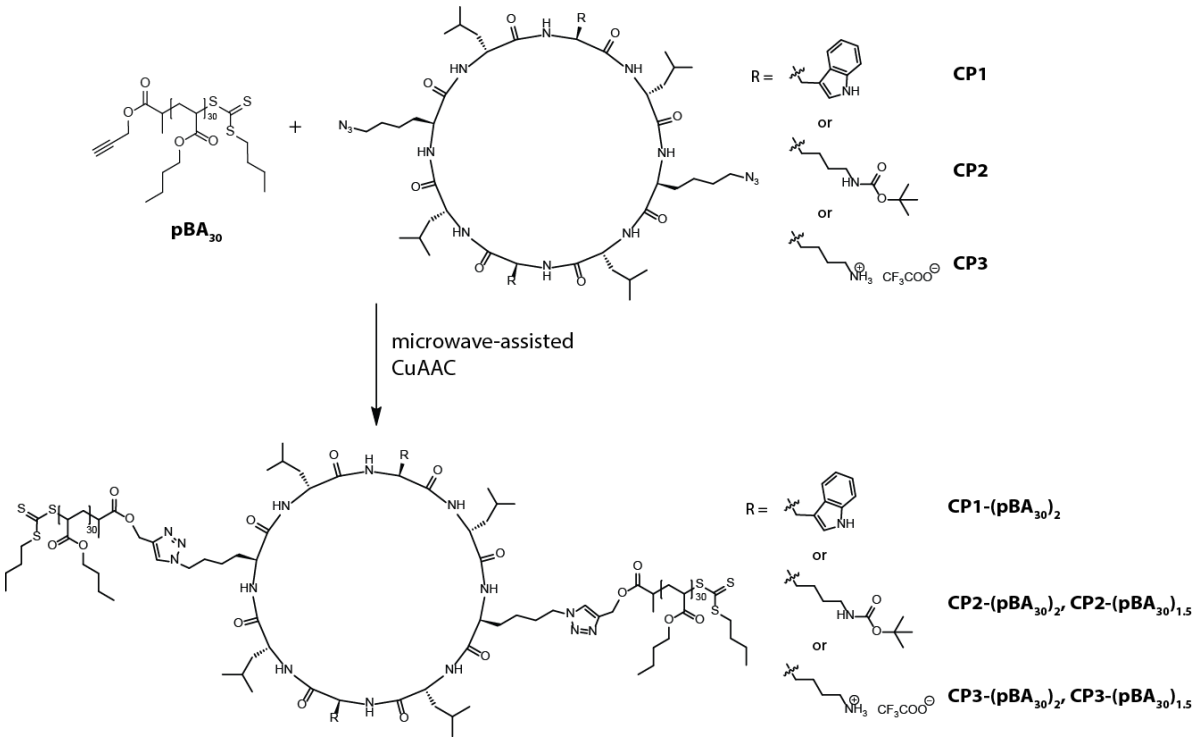

Scheme 1: Synthetic overview of cyclic peptides and (cyclic peptide)-polymer conjugates.

Influence of polymer conjugation

First we examined cyclo[(Lys(N_3)-D-Leu-Trp-D-Leu-)$_2$] **CP1**, which has two azide containing residues (incorporated to enable the introduction of two polymer chains with alkyne end groups). A very limited range of solvents can be used to obtain macroscopically clear solutions (i.e. submicron sizes) of unconjugated **CP1**, and trifluoroacetic acid (TFA) and dimethylsulfoxide (DMSO) are commonly used solvents to dissolve CPs containing these

residues.[28,29,55-57] Small angle neutron scattering (SANS) enabled direct analysis of the macroscopically dissolved **CP1** in TFA-*d* and DMSO-d_6 (Figure 1).

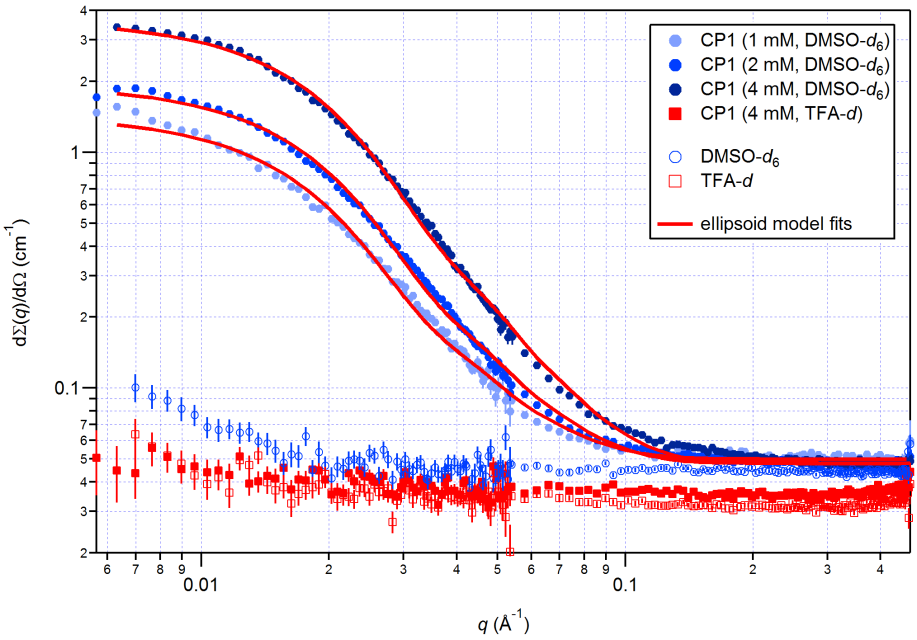

Figure 1: SANS data of **CP1** in TFA-*d* and DMSO-d_6. **CP1** is molecularly dissolved in TFA-*d* but forms 1-15 nm structures in DMSO-d_6. The figure shows the fit of a uniform ellipsoid model (disk-like) to **CP1** in DMSO-d_6 (4 mM). This has been interpreted as bundles of short tubes in DMSO-d_6. See Figures S1-S3 for model fitting.

In TFA-*d*, **CP1** does not scatter above the background incoherent scattering from the solvent. This suggests that any structure in solution is smaller than 1 nm, corresponding to the molecular dissolution of **CP1**. On the other hand, **CP1** in DMSO-d_6 shows significant small-angle scattering over the probed *q*-range, which increases with concentration, indicating the presence of small aggregates. These scattering functions were inconsistent with spherical aggregates, but could be adequately fit by models with disk-like geometry such as homogeneous oblate spheroids or cylinders. Best fit parameters are similar for the two models, yielding short cylinders with radii of 12±0.5 nm and lengths of 4.0 nm, or spheroids with large radii of 13±0.5 nm and short (axial) radii of 2.3 nm, very close to half the best-fit cylinder length. Including polydispersity into the cylinder radius improves the fit slightly but does not affect cylinder length (see Figures S1-S3 for further details).[51] These dimensions are larger than expected for a single **CP1** nanotube (which would have a radius ~ 0.5 nm), but in line with earlier observations by Ghadiri *et al*. who observed electron (and optical) microscopy images of unconjugated CPs in bundles (microcrystals).[17,56,58] We interpret the

SANS patterns to mean that **CP1** exists as bundles of short tubes in DMSO-d_6, a concept that has also been proposed in the study of CP ion channel mechanism.[59-61] Indeed, while early work in the field presented the mechanism of ion transport through the internal cavities of cyclic peptide nanotubes,[62,63] assembly into 'barrel and stave' structures has also been suggested.[64] Furthermore, the work of Ramesh *et al*. and Kodama *et al*. have shown that the transport of ions is possible with cyclic peptides with only 4 or 6 residues, for which the internal pore is too small to allow ion transport, thus suggesting a barrel and stave assembly.[59-61]

Using microwave-assisted CuAAC, we conjugated **CP1** with two chains of alkyne-functionalised poly(*n*-butyl acrylate) (**pBA_{30}**; M_n 4100 g.mol^{-1}, $Đ$ 1.16) yielding **CP1-(pBA_{30})$_2$** (Scheme 1). We probed the effect of the solvent environment on the assembly of the (cyclic peptide)-polymer conjugates, using a variety of solvents and mixtures to empirically correlate the influence of the solvent H-bonding strength in competition with H-bonding between CPs, and the solvent quality towards the peptide and polymer.

Remarkably, unlike **CP1**, the peptide-polymer conjugate **CP1-(pBA_{30})$_2$** in TFA-*d* shows an assembly of appreciable size by SANS (Figure 2). This is likely due to the polymer shielding the peptide from the TFA-*d* molecules, a phenomenon observed in a previous study.[43] This scattering pattern can also be fit to short cylinders. Here the best fit cylinder radius is 1.4 nm and length 6.5 nm (note, a fit to prolate ellipsoids gives comparable radii of 1.5 nm and 4.2 nm, respectively, see Figures S4-S5). This cylinder radius is greater than expected for the cyclopeptide alone, but is consistent with expectations for an isolated CP nanotube surrounded by a polymer sheath swollen by solvent. More complex models, to account for a solvent-penetrable polymer shell, were not necessary to fit the data; however the obtained radii and scattering length densities (SLDs) must be interpreted as an average of the peptide core and solvated polymer shell. The fact that the obtained radius is only slightly larger than expected for a single, unconjugated cyclic peptide nanotube and does not account for the full length of the polymer chain, shows not only the low contrast of the polymer but is also evidence of isolated cyclic peptide nanotubes that are sterically stabilised by the polymer chains. These findings match previous SANS analyses performed on these systems.[43]

CP1-(pBA_{30})$_2$ was difficult to dissolve in DMSO-d_6, and this is clearly seen in the q^{-4} scattering behaviour in Figure 2 at low q (< 0.03 Å^{-1}) corresponding to Porod scattering by large particles (> 100 nm).[65,66] This is consistent with the poor solubility of pBA in DMSO being carried over to the conjugate. However SANS reveals a coexistence of precipitate with a population of small, low aspect ratio aggregates in DMSO-d_6, despite the incompatibility

between DMSO-d_6 and the pBA chains. These aggregates are comparable in their dimensions with those seen in TFA. A cylinder fit yields a radius of 1 nm and a length of 6 nm, (or radii of 1 nm and 4 nm for a prolate spheroid). Here also the assemblies are short, and consistent with isolated nanotubes sterically stabilised by the polymer conjugate, and very different from the cyclopeptide **CP1** alone.

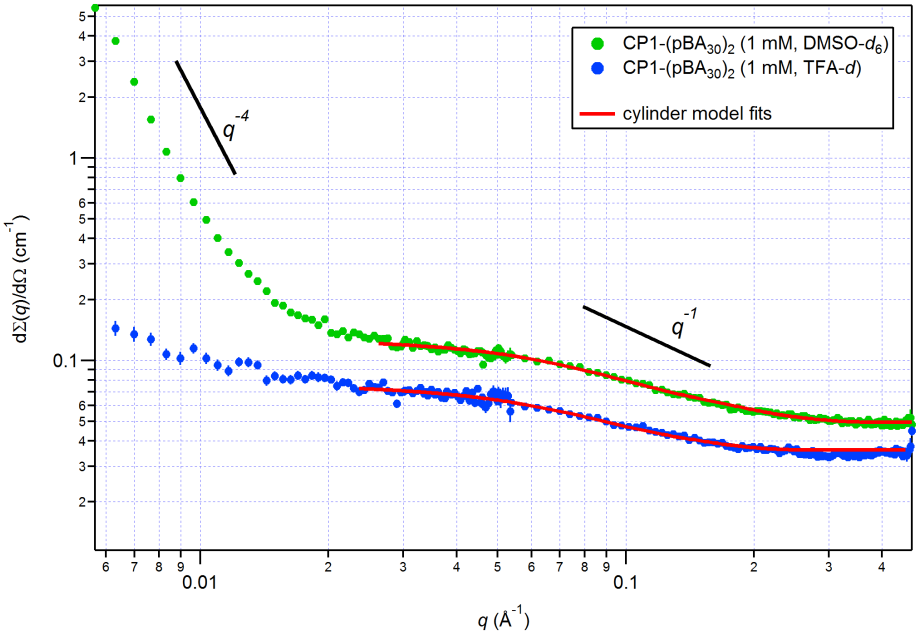

Figure 2: SANS data of **CP1-(pBA$_{30}$)$_2$** in TFA-*d* and DMSO-d_6. **CP1-(pBA$_{30}$)$_2$** exists as short individual tubes. Precipitation is observed for the conjugate in DMSO-d_6. See Figures S4-S5 for model fitting.

Influence of solvent

Since the conjugation of a polymer provides solvent solubility to the nanotubes, the conjugate **CP1-(pBA$_{30}$)$_2$** was dissolved in tetrahydrofuran-d_8 (THF-d_8) and chloroform-*d* ($CDCl_3$). In these less competitive solvents, H-bonding between CPs is promoted, and the SANS patterns exhibit a q^{-1} power law of over a wide q-range (Figure 3), characteristic of long rigid rods. This observation is consistent with previously reported electron microscopy imaging of chemically locked-in CP-polymer conjugates.[39,43] With no Guinier regime in the available q range, fitting the data gave cylinders with very high aspect ratios, with a lower bound on the average length >110 nm, and a cylinder radius of ~ 1 nm in both solvents (Figure S6). Even at very low q (0.001 Å^{-1}) the q^{-1} behaviour persists in the scattering data (Figure 4) showing the rods to be extremely long and rigid, raising the minimum observed length of the assembly to 1700 nm. Such long assemblies support the notion of a cooperative

assembly mechanism,[67] which has been suggested to originate from the stabilisation of multiple bonds and peptide backbone conformation.[56,68] The number- and weight- average degree of polymerisation, $\langle \mathrm{DP} \rangle_\mathrm{n}$ and $\langle \mathrm{DP} \rangle_\mathrm{w}$ respectively, of a supramolecular assembly with a single nucleation step can be described by:[69]

$$\langle \mathrm{DP} \rangle_\mathrm{n} = \frac{\sigma + (1-\sigma)(1-K[\mathrm{A}])^2}{\sigma(1-K[\mathrm{A}]) + (1-\sigma)(1-K[\mathrm{A}])^2} \quad (1)$$

$$\langle \mathrm{DP} \rangle_\mathrm{w} = \frac{\sigma(1+K[\mathrm{A}]) + (1-\sigma)(1-K[\mathrm{A}])^3}{\sigma(1-K[\mathrm{A}]) + (1-\sigma)(1-K[\mathrm{A}])^3} \quad (2)$$

Where $\sigma = K_2/K$; [A] is the concentration of unassembled monomer, K_2 is the equilibrium constant for the dimerization of two monomers, and K is the equilibrium constant for the addition of one monomer to an assembly with two units or more. Based on thermodynamic studies of partially *N*-methylated CPs (monotopic species), the highest equilibrium constants for the formation of dimers have been found to be in the order of 2000 M^{-1} in $CDCl_3$.[70] For an isodesmic supramolecular polymerisation (i.e. $K_2 = K$) with association constant $K \sim 2000\ M^{-1}$ at 1 mM, we calculate a weight average degree of polymerisation $<DP>_w \sim 3$ (length ~ 1.5 nm†).[69] This is significantly shorter than the assembly observed by SANS; in fact, $K \sim 10^7\ M^{-1}$ is required to explain the observed minimum length through an isodesmic growth mechanism. If we however assume a cooperative growth mechanism (in the simplest case of a nucleation step at two units, i.e. $K_2 < K$) and an association constant for the first two units of the assembly $K_2 \sim 2000\ M^{-1}$, then to obtain a $<DP>_w \sim 220$ (length ~ 110 nm†) we can estimate the equilibrium constant for subsequent growth K to be greater than 200 000 M^{-1} in $CDCl_3$ (Figure 5). If we consider longer assemblies (length ~ 1700 nm, $<DP>_w \sim 3400$†) such as those observed in THF, and with the continued assumption of $K_2 \sim 2000\ M^{-1}$, then we estimate $K \sim 1\ 200\ 000\ M^{-1}$ (Figure 5).

† A length of 5 Å per unit[17] has been used to estimate the length of assembly from DP.

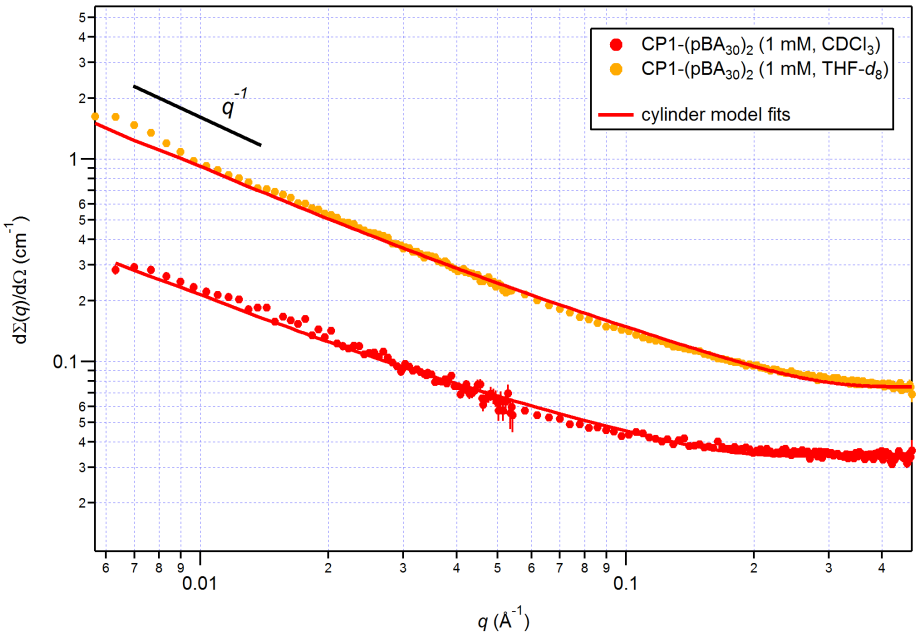

Figure 3: SANS data of **CP1-(pBA$_{30}$)$_2$** in $CDCl_3$ and THF-d_8. Conjugate exists as long and individual tubes. See Figure S6 for model fitting.

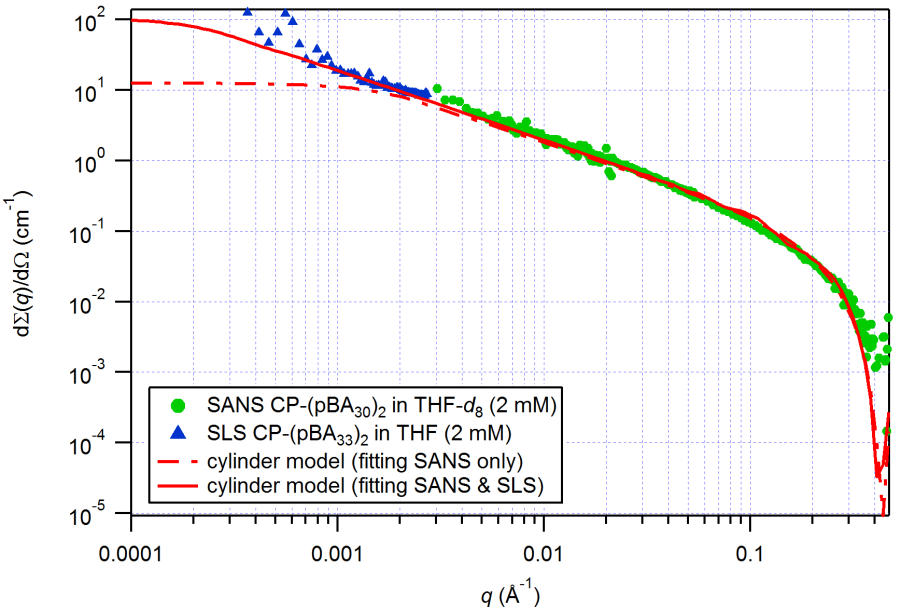

	(a) SANS only	(b) SANS and SLS overlayed
Scale	0.019†	0.019†
Radius (Å)	8.87	9.10
Length (Å)	>2100	>17000
SLD cylinder ($\times 10^{-6}$ Å^{-2})	2.70	2.80
SLD solvent ($\times 10^{-6}$ Å^{-2})	6.35†	6.35†

Figure 4: Uniform cylinder model fits to SANS data of (a) **CP1-(pBA$_{30}$)$_2$** in THF-d_8 (2 mM); and (b) **CP-(pBA$_{33}$)$_2$** in THF (2 mM). Incoherent background scattering has been subtracted. SLS data has been offset to match the SANS data. (†=held parameter value)

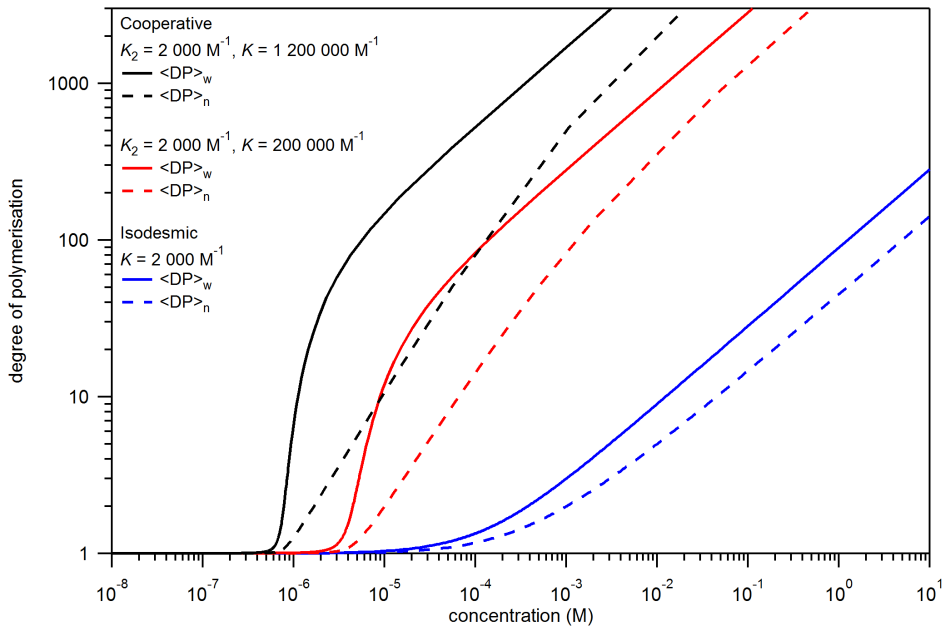

Figure 5: Calculated number- and weight-average degree of polymerisation <DP>$_n$ and <DP>$_w$ versus total concentration of CP units for isodesmic (blue lines) and cooperative growth mechanisms, with $\sigma = 0.01$ (red lines) and $\sigma = 0.0016$ (black lines).[69] A cooperative growth mechanism is used to explain the long assembly.

To probe solvent conditions with properties between those of TFA and THF or $CDCl_3$, solvent mixtures of TFA-*d*/THF-d_8 and TFA-*d*/$CDCl_3$ were used. Table 1 shows the results of these experiments (see Figures S4-9 for scattering profiles and model fitting). With only 10 vol% TFA-*d*, the assemblies are found to be significantly shorter than those observed in either neat THF-d_8 or $CDCl_3$ and yield comparable dimensions to our previous findings with the same solvent composition.[43] A closer look at the fitted parameters for radius and contrast of **CP1-(pBA$_{30}$)$_2$** in the pure solvents suggests that the polymer chains are better solvated in $CDCl_3$ (larger radius and lower contrast against solvent) than in THF-d_8 (smaller radius and higher contrast). Note that this comparison was made by fixing the scale, for the fitting, according to the volume fraction of each sample. As a cooperative system with the observed lengths, it is reasonable to assume that the entire sample is contributing to the scattering (as the unassembled species is at least 3 orders of magnitude lower than the total concentration). The difference in solvation means that TFA can more easily access the CP and disrupt its stacking when mixed with $CDCl_3$ than THF-d_8, which explains the observed differences in assembly lengths between TFA-*d*/THF-d_8 (1:9 v/v) and TFA-*d*/$CDCl_3$ (1:9 v/v). To probe this, **CP1-(pBA$_{30}$)$_2$** was dissolved first into TFA-*d*, then diluted with THF-d_8 to a final concentration and solvent mixture of TFA-*d*/THF-d_8 (10 vol%). In this case

even shorter tubes were observed, leading to the conclusion that a non-thermodynamic product is formed in one or other addition sequence (Figure S9). The details of this require further study, but do suggest the potential for obtaining kinetic products in order to access a wider range of structures.[71,72]

Table 1: Length parameter from fitting uniform cylinder model to scattering profiles of **CP1-(pBA$_{30}$)$_2$** at 1 mM in various solvent mixtures. See Figures S4-9 for scattering profiles and model fitting.

Composition of TFA-*d* (vol%)	100	90	10	0
Length in TFA-*d*/THF-d_8 (nm)	10	10	30	>110
Length in TFA-*d*/$CDCl_3$ (nm)	10	10	10	>110

Influence of cyclic peptide side-chain functionality

A key feature of using self-assembling cyclic peptides is their versatility in chemical functionality by the inclusion of residues with various functional groups. Here we use **CP2**, which substitutes (from **CP1**) the two Trp residues for two Lys(Boc) residues, as a model compound that might be potentially used to functionalise the immediate shell of a tube (i.e. conjugated to the peptide and not the polymer). Attempts to conjugate **pBA$_{30}$** to **CP2** by microwave-assisted CuAAC resulted in conversion < 100 % as judged by ATR-FTIR (Figure S10). We attribute this difference in conjugation efficiency to the bulky Boc protecting groups which reduce the accessibility of the sites (based on our findings of attempting to conjugate 4 polymers to a CP with 4 azide sites).[29] Conjugation efficiency of **pBA$_{30}$** to Boc-deprotected **CP2**, i.e. **CP3**, was difficult to ascertain due to the relative insolubility of **CP3** which biased the observation of the conjugate. Our uncertainty with conversion led us to synthesise samples where the cyclic peptide was in excess over the polymer during conjugation, to determine whether a higher number of unconjugated sites would impact the assembly. Conjugates **CP2-(pBA$_{30}$)$_2$**, **CP2-(pBA$_{30}$)$_{1.5}$** (2.1 eq and 1.5 eq of polymer used, respectively) and **CP3-(pBA$_{30}$)$_2$**, **CP3-(pBA$_{30}$)$_{1.5}$** (2.1 eq and 1.5 eq of polymer used, respectively) in $CDCl_3$ were examined by SANS to assess the impact of changing residue function on the CP assembly (Figure 6). It is clear from the scattering profiles that the structures of these two conjugates differ from the **CP1** based conjugates. The scattering patterns are all consistent with extended, anisotropic structures, and can all be fit satisfactorily by rigid rod models (Figure 6). At wavevectors ($q < 0.03$ Å^{-1}), **CP2**-based conjugates show a trend towards the expected q^{-1} power law of rigid rods (see Figure S11 for model fitting), but the steep region indicates much larger cylinder radii than **CP1**-derived

aggregates. This has been modelled by including polydispersity in the radial component *via* a Schultz distribution with a fitted polydispersity of *ca.* 1.0 (see Figure S12 for model fitting). We interpret this to be a result of the incomplete conjugation and the consequent tendency of the tubes to partially bundle. This value of radial polydispersity is reasonable as the aggregation of even two tubes will be statistically significant when compared to an isolated nanotube.

The scattering patterns of **CP3** conjugates at both grafting densities are similar to **CP1-(pBA$_{30}$)$_2$** in the intermediate *q* range, which indicates the presence of isolated cylinders. However a transition to Porod scattering is seen at lower *q*, indicative of large particles or precipitates.[65,66] This could be the result of the use and incompatibility of $CDCl_3$ as the solvent and the polar nature of the lysine residues in the **CP3** conjugates. Also of note, in both **CP2** and **CP3** conjugates, the difference between using 2.1 and 1.5 equivalents of polymer per CP during the conjugation reaction has a minimal impact on the final assembly. For conjugations involving **CP2**, this suggests a maximum grafting efficiency of 1.5 polymers per CP.

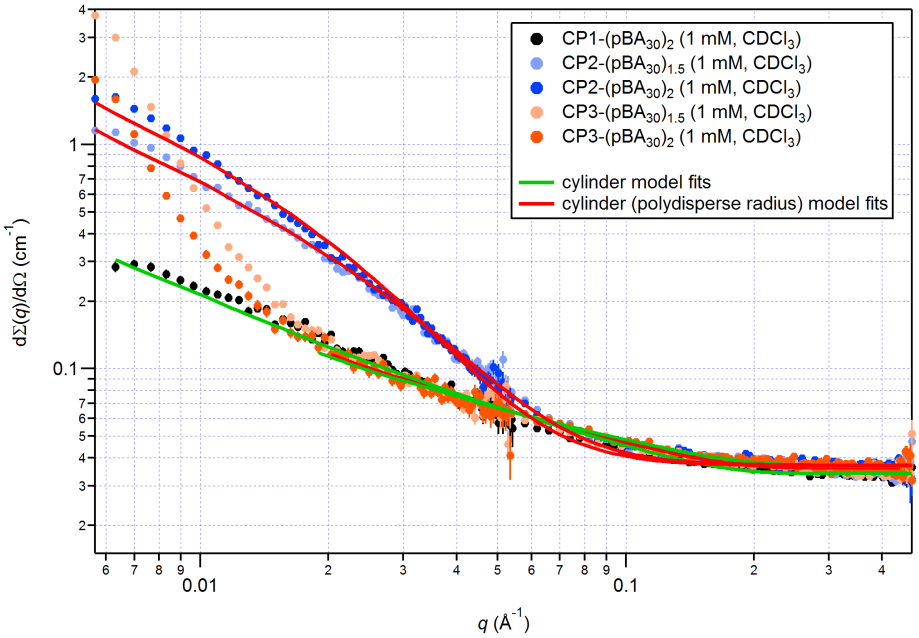

Figure 6: SANS data of **CP1-(pBA$_{30}$)$_2$**, **CP2-(pBA$_{30}$)$_2$**, **CP2-(pBA$_{30}$)$_{1.5}$**, **CP3-(pBA$_{30}$)$_2$**, **CP3-(pBA$_{30}$)$_{1.5}$**, in $CDCl_3$. Variation of peptide and variation of polymer equivalents used during conjugation. See Figure S11-S12 for model fitting.

Conclusion

We have shown the direct characterisation of nanotube forming (cyclic peptide)-polymer conjugates in a variety of conditions. These conditions and self-assembly products have been summarised in Scheme 2. Fitting the form factor with cylindrical models suggests the attachment of pBA can sterically stabilise these assemblies, preventing the formation of bundles as otherwise observed in the assembly of the unconjugated cyclic peptide in DMSO-d_6. Interestingly, in the case of the conjugate in DMSO-d_6, large structures were also observed to coexist with isolated nanotubes; this complex behaviour is likely to be related to the incompatibility (i.e. low solubility) of pBA with DMSO. In TFA-*d*, where there was no assembly of the unconjugated cyclic peptide, the polymer promoted the formation of (short) nanotubes in the conjugate, a phenomenon we have attributed to the polymer chains shielding the solvent from the CP hydrogen bond donors and acceptors. This notion was further explored by using solvent mixtures varying in their ability to compete with the H-bonding between CPs. It was found that 10 vol% TFA-*d* was enough to significantly shorten the length of the assembly from a non-polar solvent. CP-pBA conjugates in THF were found to exist as individual and long (> 1700 nm) nanotubes; which, by extension of the observed length and concentration, suggests a strongly cooperative system where we estimate for nucleation $K_2 = 2000\ \mathrm{M}^{-1}$, and for elongation $K > 1\ 200\ 000\ \mathrm{M}^{-1}$ as a minimum for cooperative growth to explain the observations. We explored the variation of residues of the CP from Trp to Lys(Boc) or Lys, where an observable difference was found between the resulting self-assembled structure for each of these species. Specifically, the incomplete conjugation due to Lys(Boc) residues led to partial lateral aggregation; in the case of Lys residues, while unbundled nanotubes were observed, aggregates were also present in $CDCl_3$ which have been attributed to the polar nature of the Lys residues.

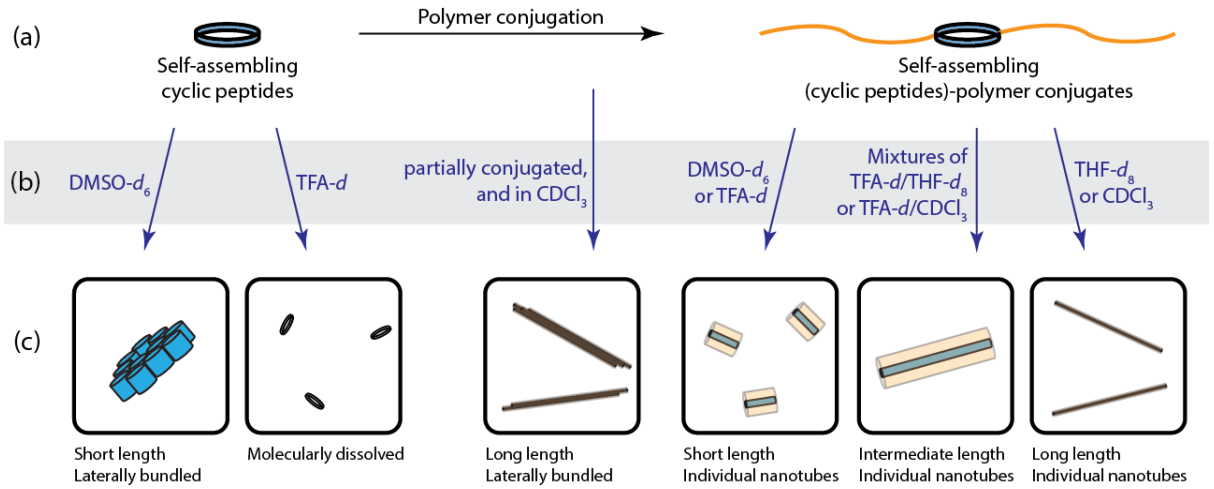

Scheme 2: Simplified summary depicting: (a) self-assembling units, (b) key assembly conditions, and (c) products of self-assembly with short descriptions below. Length scales and concentrations have not been correctly represented for the purpose of illustration.

Acknowledgements

The authors acknowledge Robert Chapman (Sydney) for providing pBA_{30}; Philip G. Young (Sydney) for providing $DMTMM.BF_4$; Algi Serelis (DuluxGroup, Australia) for providing PABTC; and Sophie Larnaudie (Warwick) for providing $DMTMM.BF_4$ and NHS-PABTC. The authors thank Paul Butler (NIST) for support with the SANS experiments.

The Australian Research Council Discovery (DP140100241; K.A.J. and S.P.) Programme is acknowledged for funding. M.L.K. acknowledges the Australian Government for the provision of an Australian Postgraduate Award research scholarship. The Royal Society Wolfson Merit Award (WM130055; SP) and the Monash-Warwick Alliance (MLK) are acknowledged for financial support.

We acknowledge the support of the National Institute of Standards and Technology, U.S. Department of Commerce, in providing the neutron research facilities used in this work. This work utilized facilities supported in part by the National Science Foundation under Agreement No. DMR-0944772.

References

[1] Gao, X.; Matsui, H. *Advanced Materials* **2005**, *17*, 2037-2050.
[2] de la Rica, R.; Pejoux, C.; Matsui, H. *Advanced Functional Materials* **2011**, *21*, 1018-1026.
[3] Martin, C. R.; Kohli, P. *Nature Reviews Drug Discovery* **2003**, *2*, 29-37.
[4] Scanlon, S.; Aggeli, A. *Nano Today* **2008**, *3*, 22-30.
[5] Shimizu, T.; Masuda, M.; Minamikawa, H. *Chemical Reviews* **2005**, *105*, 1401-1443.
[6] Couet, J.; Biesalski, M. *Soft Matter* **2006**, *2*, 1005-1014.
[7] Huang, K.; Rzayev, J. *Journal of the American Chemical Society* **2009**, *131*, 6880-6885.
[8] Zhang, M.; Müller, A. H. E. *Journal of Polymer Science Part A: Polymer Chemistry* **2005**, *43*, 3461-3481.
[9] Sheiko, S. S.; Sumerlin, B. S.; Matyjaszewski, K. *Progress in Polymer Science* **2008**, *33*, 759-785.
[10] Tasis, D.; Tagmatarchis, N.; Bianco, A.; Prato, M. *Chemical Reviews* **2006**, *106*, 1105-1136.
[11] Ketchem, R. R.; Hu, W.; Cross, T. A. *Science* **1993**, *261*, 1457-1460.
[12] Ketchem, R. R.; Roux, B.; Cross, T. A. *Structure* **1997**, *5*, 1655-1669.
[13] Song, L.; Hobaugh, M. R.; Shustak, C.; Cheley, S.; Bayley, H.; Gouaux, J. E. *Science* **1996**, *274*, 1859-1865.
[14] Klug, A. *Angewandte Chemie International Edition in English* **1983**, *22*, 565-582.
[15] Namba, K.; Pattanayek, R.; Stubbs, G. *Journal of Molecular Biology* **1989**, *208*, 307-325.
[16] Aida, T.; Meijer, E. W.; Stupp, S. I. *Science* **2012**, *335*, 813-817.
[17] Ghadiri, M. R.; Granja, J. R.; Milligan, R. A.; McRee, D. E.; Khazanovich, N. *Nature* **1993**, *366*, 324-327.
[18] Brea, R. J.; Reiriz, C.; Granja, J. R. *Chemical Society Reviews* **2010**, *39*, 1448-1456.
[19] Chapman, R.; Danial, M.; Koh, M. L.; Jolliffe, K. A.; Perrier, S. *Chemical Society Reviews* **2012**, *41*, 6023-6041.
[20] Mizrahi, M.; Zakrassov, A.; Lerner-Yardeni, J.; Ashkenasy, N. *Nanoscale* **2012**, *4*, 518-524.
[21] García-Fandiño, R.; Granja, J. R. *The Journal of Physical Chemistry C* **2013**, *117*, 10143-10162.
[22] Vandermeulen, G. W. M.; Klok, H.-A. *Macromolecular Bioscience* **2004**, *4*, 383-398.
[23] Klok, H. A. *Journal of Polymer Science Part A: Polymer Chemistry* **2005**, *43*, 1-17.
[24] Börner, H. G. *Progress in Polymer Science* **2009**, *34*, 811-851.
[25] Couet, J.; Jeyaprakash, J. D.; Samuel, S.; Kopyshev, A.; Santer, S.; Biesalski, M. *Angewandte Chemie International Edition* **2005**, *44*, 3297-3301.
[26] ten Cate, M. G. J.; Severin, N.; Börner, H. G. *Macromolecules* **2006**, *39*, 7831-7838.
[27] Chapman, R.; Jolliffe, K. A.; Perrier, S. *Australian Journal of Chemistry* **2010**, *63*, 1169-1172.
[28] Chapman, R.; Jolliffe, K. A.; Perrier, S. *Polymer Chemistry* **2011**, *2*, 1956-1963.
[29] Poon, C. K.; Chapman, R.; Jolliffe, K. A.; Perrier, S. *Polymer Chemistry* **2012**, *3*, 1820-1826.
[30] Loschonsky, S.; Couet, J.; Biesalski, M. *Macromolecular Rapid Communications* **2008**, *29*, 309-315.
[31] Hourani, R.; Zhang, C.; van der Weegen, R.; Ruiz, L.; Li, C.; Keten, S.; Helms, B. A.; Xu, T. *Journal of the American Chemical Society* **2011**, *133*, 15296-15299.
[32] Li, L. S.; Zhan, H.; Duan, P.; Liao, J.; Quan, J.; Hu, Y.; Chen, Z.; Zhu, J.; Liu, M.; Wu, Y.-D.; Deng, J. *Advanced Functional Materials* **2012**, *22*, 3051-3056.

[33] Chapman, R.; Warr, G. G.; Perrier, S.; Jolliffe, K. A. *Chemistry – A European Journal* **2013**, *19*, 1955-1961.
[34] Chapman, R.; Bouten, P. J. M.; Hoogenboom, R.; Jolliffe, K. A.; Perrier, S. *Chemical Communications* **2013**, *49*, 6522-6524.
[35] Danial, M.; Tran, C. M. N.; Jolliffe, K. A.; Perrier, S. *Journal of the American Chemical Society* **2014**, *136*, 8018-8026.
[36] Wang, Y.; Yi, S.; Sun, L.; Huang, Y.; Lenaghan, S. C.; Zhang, M. *Journal of Biomedical Nanotechnology* **2014**, *10*, 445-454.
[37] Blunden, B. M.; Chapman, R.; Danial, M.; Lu, H.; Jolliffe, K. A.; Perrier , S.; Stenzel, M. H. *Chemistry – A European Journal* **2014**, doi: 10.1002/chem.201403130.
[38] Couet, J.; Biesalski, M. *Small* **2008**, *4*, 1008-1016.
[39] Chapman, R.; Jolliffe, K. A.; Perrier, S. *Advanced Materials* **2013**, *25*, 1170-1172.
[40] Xu, T.; Zhao, N.; Ren, F.; Hourani, R.; Lee, M. T.; Shu, J. Y.; Mao, S.; Helms, B. A. *ACS Nano* **2011**, *5*, 1376-1384.
[41] Danial, M.; My-Nhi Tran, C.; Young, P. G.; Perrier, S.; Jolliffe, K. A. *Nature Communications* **2013**, *4*, doi: 10.1038/ncomms3780.
[42] Gokhale, R.; Couet, J.; Biesalski, M. *Physica Status Solidi A: Applications and Materials Science* **2010**, *207*, 878-883.
[43] Chapman, R.; Koh, M. L.; Warr, G. G.; Jolliffe, K. A.; Perrier, S. *Chemical Science* **2013**, *4*, 2581-2589.
[44] Goddard-Borger, E. D.; Stick, R. V. *Organic Letters* **2007**, *9*, 3797-3800.
[45] Goddard-Borger, E. D.; Stick, R. V. *Organic Letters* **2011**, *13*, 2514-2514.
[46] Raw, S. A. *Tetrahedron Letters* **2009**, *50*, 946-948.
[47] Merrifield, R. B. *Journal of the American Chemical Society* **1963**, *85*, 2149-2154.
[48] Fields, G. B.; Noble, R. L. *International Journal of Peptide and Protein Research* **1990**, *35*, 161-214.
[49] Moss, J. A. *Current Protocols in Protein Science* **2005**, 18.17.11-18.17.19.
[50] Konkolewicz, D.; Gray-Weale, A.; Perrier, S. *Journal of the American Chemical Society* **2009**, *131*, 18075-18077.
[51] Kline, S. *Journal of Applied Crystallography* **2006**, *39*, 895-900.
[52] Sears, V. F. *Neutron News* **1992**, *3*, 26-37.
[53] NCNR Scattering Length Density Calculator, http://www.ncnr.nist.gov/resources/sldcalc.html (accessed 2013)
[54] Zemb T.; Linder, P. *Neutrons, X-rays and Light: Scattering Methods Applied to Soft Condensed Matter*; Elsevier, **2002**.
[55] Clark, T. D.; Buehler, L. K.; Ghadiri, M. R. *Journal of the American Chemical Society* **1998**, *120*, 651-656.
[56] Hartgerink, J. D.; Granja, J. R.; Milligan, R. A.; Ghadiri, M. R. *Journal of the American Chemical Society* **1996**, *118*, 43-50.
[57] Kim, H. S.; Hartgerink, J. D.; Ghadiri, M. R. *Journal of the American Chemical Society* **1998**, *120*, 4417-4424.
[58] Khazanovich, N.; Granja, J. R.; McRee, D. E.; Milligan, R. A.; Ghadiri, M. R. *Journal of the American Chemical Society* **1994**, *116*, 6011-6012.
[59] Suga, T.; Osada, S.; Kodama, H. *Bioorganic & Medicinal Chemistry* **2012**, *20*, 42-46.
[60] Taira, J.; Osada, S.; Hayashi, R.; Ueda, T.; Jelokhani-Niaraki, M.; Aoyagi, H.; Kodama, H. *Bulletin of the Chemical Society of Japan* **2010**, *83*, 683-688.
[61] Ramesh, J.; Ghosh, J. K.; Swaminathan, C. P.; Ramasamy, P.; Surolia, A.; Sikdar, S. K.; Easwaran, K. R. K. *The Journal of Peptide Research* **2003**, *61*, 63-70.
[62] Ghadiri, M. R.; Granja, J. R.; Buehler, L. K. *Nature* **1994**, *369*, 301-304.

[63] Granja, J. R.; Ghadiri, M. R. *Journal of the American Chemical Society* **1994**, *116*, 10785-10786.
[64] Fernandez-Lopez, S.; Kim, H. S.; Choi, E. C.; Delgado, M.; Granja, J. R.; Khasanov, A.; Kraehenbuehl, K.; Long, G.; Weinberger, D. A.; Wilcoxen, K. M.; Ghadiri, M. R. *Nature* **2001**, *412*, 452-455.
[65] Porod, G. *Kolloid-Zeitschrift* **1951**, *124*, 83-114.
[66] Porod, G. in *Small Angle X-ray Scattering*; O. Glatter, O. Kratky, Eds.; Academic Press: London, **1982**.
[67] De Greef, T. F. A.; Smulders, M. M. J.; Wolffs, M.; Schenning, A. P. H. J.; Sijbesma, R. P.; Meijer, E. W. *Chemical Reviews* **2009**, *109*, 5687-5754.
[68] Ghadiri, M. R.; Kobayashi, K.; Granja, J. R.; Chadha, R. K.; McRee, D. E. *Angewandte Chemie International Edition* **1995**, *34*, 93-95.
[69] Zhao, D.; Moore, J. S. *Organic & Biomolecular Chemistry* **2003**, *1*, 3471-3491.
[70] Clark, T. D.; Buriak, J. M.; Kobayashi, K.; Isler, M. P.; McRee, D. E.; Ghadiri, M. R. *Journal of the American Chemical Society* **1998**, *120*, 8949-8962.
[71] Ogi, S.; Fukui, T.; Jue, M. L.; Takeuchi, M.; Sugiyasu, K. *Angewandte Chemie International Edition* **2014**, *53*, 14363-14367.
[72] Ogi, S.; Sugiyasu, K.; Manna, S.; Samitsu, S.; Takeuchi, M. *Nature Chemistry* **2014**, *6*, 188-195.